Electronic Structure of Spatially Aligned Graphene Nanoribbons on Au(788)

S. Linden,[1] D. Zhong,[1] A. Timmer,[1] N. Aghdassi,[1] J. H. Franke,[1] H. Zhang,[1] X. Feng,[2] K. Müllen,[2] H. Fuchs,[1,3] L. Chi,[1] and H. Zacharias[1]

[1]*Physikalisches Institut, Westfälische Wilhelms-Universität, Wilhelm-Klemm Strasse 10, and Center for Nanotechnology, Heisenbergweg 11, 48149 Münster, Germany*

[2]*Max-Planck-Institut for Polymer Research, Ackermannweg 10, 55128 Mainz, Germany*

[3]*Institute for Nanotechnology, Karlsruhe Institute of Technology, 76344 Karlsruhe, Germany*

(Received 20 January 2012; published 21 May 2012)

We report on a bottom-up approach of the selective and precise growth of subnanometer wide straight and chevron-type armchair nanoribbons (GNRs) on a stepped Au(788) surface using different specific molecular precursors. This process creates spatially well-aligned GNRs, as characterized by STM. High-resolution direct and inverse photoemission spectroscopy of occupied and unoccupied states allows the determination of the energetic position and momentum dispersion of electronic states revealing the existence of band gaps of several electron volts for straight 7-armchair, 13-armchair, and chevron-type GNRs in the electronic structure.

DOI: 10.1103/PhysRevLett.108.216801 PACS numbers: 73.22.Pr, 68.65.Pq, 79.60.Jv

The remarkable structural and electronic properties of graphene have stimulated intense research on its basic properties as well as on possible promising applications [1]. The behavior of the charge carriers as massless Dirac fermions near the Fermi level and the ballistic charge transport in graphene stimulate expectations to use it as a building block in electronic devices. Ideal graphene lacks, however, a band gap and is therefore semimetallic making electronic control of the conductance, the basic concept of integrated electronics, difficult. A band gap opening is expected for adsorbate modified graphene [2,3] and theoretically also for laterally confined ribbons of graphene [4–8]. There, a stronger lateral confinement increases the electronic band gap. For graphene nanoribbons (GNRs) of subnanometer width sizable values of more than an electron volt are expected. The dispersion of the electronic states is determined by the specific atomic structure of the GNR, viz., its border termination, being of armchair, zigzag, or chiral type. Comparatively broad GNRs have been produced by lithographic techniques [9,10], unzipping of carbon nanotubes [11,12], and chemical synthesis [13–15]. Recently, on-surface covalent coupling of adsorbed organic precursor molecules in ultrahigh vacuum enabled the production of atomically precise graphene nanoribbons [16]. This reliable method yields a high density of nanoribbons, however, with random orientation. We present here a robust way for the production of spatially aligned GNRs of different topologies employing this bottom-up surface catalyzed growth on stepped Au(788) surfaces. From those GNRs we experimentally investigate the occupied and unoccupied states via direct and inverse photoemission experiments and demonstrate that GNRs indeed exhibit a large band gap.

Spatially aligned GNRs were prepared on clean vicinal Au(788) surfaces under ultrahigh vacuum conditions. After deposition of the primary molecules [see Figs. 1(b) and 1(e)] from quartz crucibles the surfaces was heated to 440–470 K for dehalogenization and polymerization, while cyclodehydrogenization is achieved at 590 K [16], resulting in straight 7-armchair graphene nanoribbons (7-aGNRs) and chevron-type GNRs. The structure of the

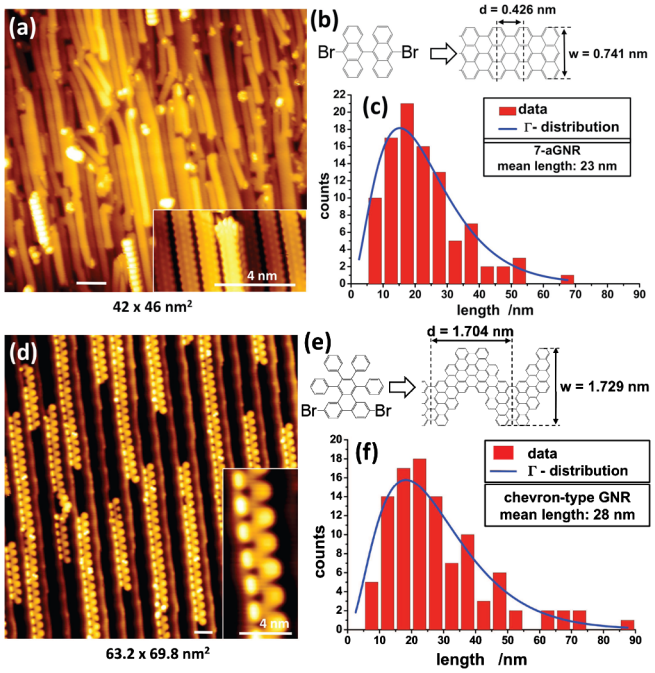

FIG. 1 (color online). STM images of aligned graphene nanoribbons (GNRs) on Au(788) surfaces. (a) Seven atoms wide straight ribbons (7-aGNR) (STM feedback 2 V/10 pA; inset: 0.1 V/0.5 nA). Scale bars: 4 nm. (b) Precursor molecule and unit cell $d = 0.426$ nm, width: $w = 0.741$ nm. (c) Distribution of the ribbon length, mean value $L = 23$ nm. (d) Chevron-type ribbons (STM feedback -2 V/50 pA; inset: 0.1 V/0.5 nA). (e) Precursor molecule and unit cell $d = 1.704$ nm, width: $w = 1.729$ nm. (f) Length distribution, mean value $L = 28$ nm.

primary molecule determines the width and the shape of the nanoribbons, and the precursors chosen here generate armchair nanoribbons. The precise alignment of the nanoribbons occurs by the template provided by the vicinal Au (788) surface, which exhibits a periodic succession of narrow terraces and parallel monatomic steps. The terraces show a {111} structure and are on average 3.83 nm wide with steps being of {111} type.

Figure 1 shows STM images of aligned GNRs at different coverages. The STM pictures indicate that the GNRs are spatially well aligned and only occasionally deviate from the general alignment along the terraces of the Au (788) substrate. For straight 7-aGNRs the atomic structure model [Fig. 1(b)] shows a width of $w = 0.741$ nm and a size of the unit cell along the ribbon of $d = 0.426$ nm, both supported by the STM images. Figure 1(c) illustrates the distribution of the length of the ribbons with a mean value of $L = 23$ nm. The structure of the chevron-type GNRs is depicted in Fig. 1(e). The overall width of the ribbon is $w = 1.729$ nm and the unit cell has a size of $d = 1.704$ nm. The STM image shown in Fig. 1(d) is intentionally prepared at a low coverage of $\Theta \sim 0.1$–0.2 monolayers, so that the Au(788) steps can be recognized. In this case a mean value of the ribbon length of $L = 28$ nm is found from Fig. 1(f), but some ribbons extend even to 90 nm and more. For both types of ribbons the length distribution can be fitted well with a gamma distribution, which supports the expectation of GNR growth being a random process. The insets in the images show GNRs at higher resolution. Remarkably, for both types of GNRs the width is extremely well defined, no deviation from the given structure is observed, unless, at high coverage, two ribbons occasionally fuse to yield one with a nearly doubled width of 13 atoms (13-aGNR). Many different samples have been prepared, all GNRs showing reproducibly the same structure and the same alignment as displayed in Figs. 1(a) and 1(d).

On these well-aligned GNRs, angle resolved UV photoemission (ARUPS) studies have been performed in both directions along the long axis of the ribbons and perpendicular to it. Figure 2 shows occupied graphene related states observed for both types of GNRs. Spectra were taken in angular steps of 1°, where zero denotes emission along the macroscopic surface normal. For straight 7-aGNRs [Fig. 2(a)], a spectral feature at about 1 eV below the Fermi level E_F appears at Γ, and slightly disperses to higher binding energies. In a peak profile analysis this feature can be decomposed into two states with binding energies of $E_{b1} = (-0.87 \pm 0.14)$ eV and $E_{b2} = (-1.21 \pm 0.16)$ eV, indicated by red and blue lines, respectively. The one at lower binding energy shows a higher intensity by a factor of 3 throughout most of the detected angular range. Both states show a similar quasifree electron dispersion with an effective mass of $m^* = (-1.07 \pm 0.17)\ m_e$. These GNR features reside on

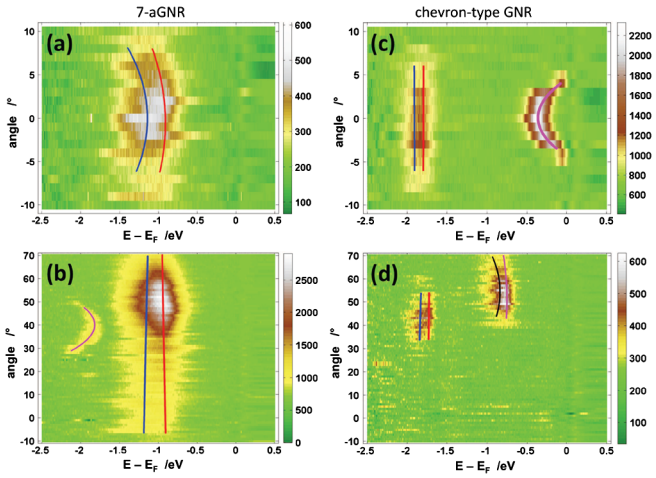

FIG. 2 (color online). Background corrected ARUPS signal for 7-aGNR (a),(b) and chevron-type (c),(d) armchair nanoribbons on Au(788) along (a),(c) and perpendicular (b),(d) to the ribbon axis. The graphs show the emission angle plotted versus the binding energy with respect to the Fermi level, while the intensity is color coded.

a background caused by the gold sp band, which after a separate measurement of the clean gold sample has been subtracted in Figs. 2(a)–2(d). In the direction perpendicular to the ribbon axis, a GNR state arises also around -1 eV binding energy. This electronic structure can be observed throughout the whole angular range measured from $\theta = -10°$ to $\theta = 70°$. It shows a pronounced intensity around $\theta = 50°$. Again this feature can be decomposed into two states with $E_{b1} = (-0.84 \pm 0.10)$ eV and $E_{b2} = (-1.19 \pm 0.17)$ eV binding energy. It is not surprising that these states do not disperse due to the localizing nature of the thin ribbon with a width of $w = 0.741$ nm. Their binding energies agree well with those observed in the direction along the ribbon axis, and it may be concluded that the same states are observed. A second spectral feature due to graphene appears in the angular range from $\theta = 25°$ to $\theta = 50°$ and a minimum binding energy of $E_{b3} = (-1.79 \pm 0.22)$ eV at $\theta = 41°$. This third state shows a free-electron-like dispersion with $m^* = -(0.83 \pm 0.07) m_e$. It may be noted that the stepped Au(788) surface besides {111} terraces shows also steps with a {111} facet. The normal of these steps encloses an angle of $\theta = 51.5°$ with the general surface normal, which may be the cause for the high emission intensity around this angle.

The chevron-type GNRs reveal two states at $E_{b3} = (-1.79 \pm 0.08)$ eV and $E_{b4} = (-1.91 \pm 0.14)$ eV along their long axis [Figs. 2(c) and 2(d)]. These states show no dispersion. Their localized nature becomes also evident in the STM images [Fig. 1(d)]. There, a high density of states is found at the lower and upper inflections of the chevron, while in between only a weak intensity is found. In the perpendicular direction [Fig. 2(d)] the same two states are observed at about the same energies within the error bars. In addition, however, at photoelectron emission

angles from $\theta = 40°$ to $\theta = 70°$ a second pair of states features a prominent signal. A deconvolution yields binding energies of $E_{b1} = (-0.72 \pm 0.13)$ eV and $E_{b2} = (-0.84 \pm 0.18)$ eV. These two states for the chevron-type and that at -1.8 eV binding energy for the 7-aGNR are only observed in the direction perpendicular to the ribbons and may be attributed to interface states. At low coverage of the surface, the Au(788) surface state at $E_b = (-0.32 \pm 0.03)$ eV is still observed [Fig. 2(c)] with a small upward shift in energy by $\Delta E = 60$ meV towards the Fermi level compared to clean Au(788) [17]. GNR states at binding energies larger than -3.5 eV are obscured in the present setup by the strong gold d bands, which begin to appear at about $E_b = -4$ eV below the Fermi level, and peak at about $E_b = -6$ eV with a relative intensity, which is higher by a factor of 260 compared to those of the GNR signals.

Unoccupied states can be investigated by inverse photoemission (IPE). Figure 3 shows IPE results for the same GNR samples, on which ARUPS was performed. After subtraction of a background due to secondary electron scattering [18] and due to the signal of the gold substrate, which is measured separately, some prominent features are observed. The straight GNRs reveal five different states [Fig. 3(a)]. From a fitting to Gaussian profiles clearly a shoulder is observed at an excitation energy of $E_u = (0.7 \pm 0.2)$ eV above Fermi, followed by a spectral feature at $E_u = (1.9 \pm 0.7)$ eV. Other states can be identified at $E_u = (3.3 \pm 0.8)$, (4.4 ± 0.5), and (5.9 ± 0.6) eV above Fermi. Since the work function is determined to be $\phi = (5.1 \pm 0.1)$ eV, the fourth state with a binding energy of $E_b = (4.4 \pm 0.5)$ eV relative to vacuum can be identified as an image state. On the chevron-type GNRs the unoccupied states are not as prominent as on the straight ones [Fig. 3(b)]. Nevertheless, features at $E_u = (1.3 \pm 0.5)$, (2.6 ± 0.9), (4.1 ± 0.7) eV, and (6.1 ± 1.9) eV above the Fermi level are present. These spectral features and especially the energetically lowest ones are fairly broad with widths of $\Delta E \sim 1.1$ eV, and 1.9 eV (FWHM). They probably consist of a superposition of several individual states.

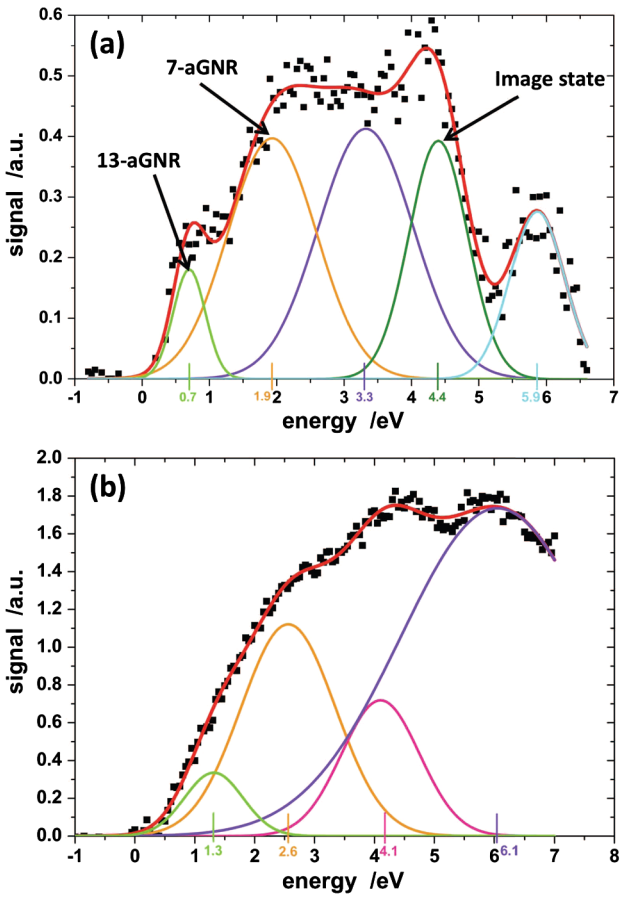

FIG. 3 (color online). IPE results for (a) 7-aGNR and 13-aGNR and (b) chevron-type GNRs.

The experimentally observed states and their dispersion can be compared to calculated band structures of nanoribbons. In Fig. 4 the experimental data for straight 7-aGNRs are compared with a band structure calculation based on density functional theory (DFT) in the local spin density approximation with gradient corrections [19,20]. The PBE functional [21] is employed along with the projector augmented-wave method [22,23] and semiempirical dispersion corrections according to Grimme [24]. At the Γ point the two highest occupied states appear in the calculation at the position of states observed experimentally. The experimental dispersion is, however, weaker than theoretically predicted for a ribbon fully saturated with hydrogen atoms at the rim. These calculations further indicate that the size of the band gap is not sensitive to the length of the GNRs. For GNRs consisting of only 12 and 14 units in length, and thus much shorter than the experimentally realized ones, the band structure follows closely that of infinite length. On the chevron-type ribbons the energetic positions of the four occupied states observed agree also very well with predicted LDA positions [16]. Dispersion is not expected to occur, as it was observed. For the unoccupied

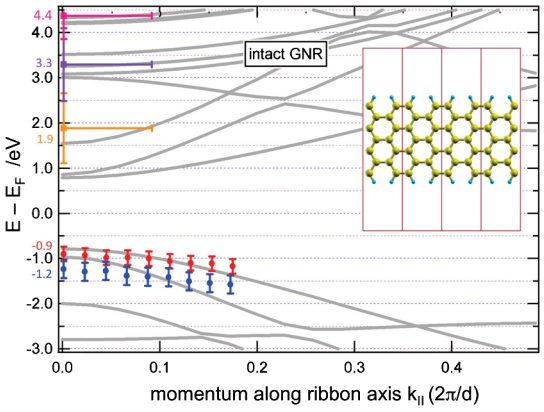

FIG. 4 (color online). Electronic band structure of the 7-aGNR along the long axis. The experimental data (colored dots with error bars) are compared to DFT local spin density approximation calculations of straight fully hydrogen saturated ribbons.

states it is evident that here only a superposition of several states has been observed and the high density of states expected theoretically cannot be resolved by IPE.

The experimentally observed energetic positions of occupied and unoccupied states can thus be combined to obtain information about the band gap in these GNRs. When the low-energy shoulder in the straight ribbons [Fig. 3(a)] is tentatively considered to be due to fused ribbons and thus 13-aGNRs, then a band gap for straight 7-aGNRs and 13-aGNRs of $E_g = (2.8 \pm 0.4)$ eV and $E_g = (1.6 \pm 0.4)$ eV, respectively, is derived. Similarly, for the chevron-type ribbons a gap of $E_g = (3.1 \pm 0.4)$ eV is obtained, if the state, which is observed only perpendicular to the ribbons and only at large emission angles, is ascribed to an interface state. Interestingly, the experimental gap for the chevron-type ribbon is much larger than that of the 13-aGNR. It seems that here not the overall width of the chevron of 1.7 nm is determining the band gap, but the strong localization at the inflections of the chevron.

These experimental data can be compared to theoretically predicted band gaps. Due to the strong localization in the ribbon, many-body electron effects become important. Quasiparticle corrections in the *GW* approximation [5,7,8] increase the gap energy significantly to 3.8 eV for 7-aGNR and 2.3 eV for 13-aGNRs. A subsequent consideration of the electron-hole interaction by solving the Bethe-Salpeter equation leads further to excitonic states with binding energies of 1.8 eV with respect to the lowest unoccupied molecular orbital [5,6,8], thus reducing the optical gap considerably. The theoretical band gaps for straight GNRs are thus larger than the experimental ones established in this work. On the other hand, the next higher unoccupied state shows in *GW* theory the same relative excitation as observed. This discrepancy could principally arise from partly dehydrogenated GNRs or from the interaction with the substrate. Since the on-surface synthesis of the GNRs is conducted at elevated substrate temperatures, ribbons with missing hydrogen atoms at the periphery might be grown. When on average one or two hydrogen atoms are missing on the ribbons, theory predicts that new states arise at somewhat larger binding energy and with a weaker dispersion. However, the highest occupied bands at the Γ point are not much affected by missing hydrogen atoms [5]. The *GW* band gap and also the exciton binding energy are reduced, leading to nearly the same gap energy and optical absorption spectrum as for fully hydrogen saturated ribbons. Only at higher $k_{\|}$ an unoccupied state dispersing to lower energies is obtained in the calculations. This excludes a possible dehydrogenization as a cause for the smaller band gap. The theoretical approaches, however, assume freestanding GNRs, while in the present case the GNRs are deposited on a gold surface. Although the electronic interaction of gold with graphene is supposed to be weak [25], the spatial alignment provided by the steps of Au(778) indicates already a finite interaction of these ribbons with the support and also among each other. The close vicinity of the metal electrons enhances the screening in the ribbons and therefore reduces the electron-electron interaction in the confined nanoribbons. This in turn leads to a reduced band gap of the GNRs on gold.

To conclude, the on-surface growth of graphene nanoribbons from molecular precursors on Au(788) produces spatially well-aligned armchair ribbons with a defined structure and a width of 0.741 and 1.729 nm for straight 7-aGNR and chevron-type GNRs, respectively. The spectroscopic identification of occupied and unoccupied electronic states on these armchair graphene nanoribbons clearly establishes a sizable electronic band gap due to the narrow width of the ribbons. The magnitude of the band gap depends on the type of the nanoribbon. The results presented yield promising perspectives for a defined nanoelectronics using narrow graphene ribbons prepared by bottom-up directed growth under well-defined conditions. The spatially precise alignment of the ribbons may allow a transfer of the prealigned graphene ribbons to other substrates, such as dielectrics.

The authors acknowledge financial support by the Deutsche Forschungsgemeinschaft via the Transregio TRR 61, "Multilevel Molecular Assemblies: Structure, Dynamics and Function" and the Priority Research Program SPP 1459, "Graphene."

[1] A. K. Geim and K. S. Novoselov, Nature Mater. **6**, 183 (2007).
[2] P. Sessi, J. R. Guest, M. Bode, and N. P. Guisinger, Nano Lett. **9**, 4343 (2009).
[3] R. Balog *et al.*, Nature Mater. **9**, 315 (2010).
[4] Y. W. Son, M. L. Cohen, and S. G. Louie, Phys. Rev. Lett. **97**, 216803 (2006).
[5] D. Prezzi, D. Varsano, A. Ruini, A. Marini, and E. Molinari, Phys. Rev. B **77**, 041404 (2008).
[6] L. Yang, M. L. Cohen, and S. G. Louie, Nano Lett. **7**, 3112 (2007).
[7] L. Yang, C. H. Park, Y. W. Son, M. L. Cohen, and S. G. Louie, Phys. Rev. Lett. **99**, 186801 (2007).
[8] D. Prezzi, D. Varsano, A. Ruini, and E. Molinari, Phys. Rev. B **84**, 041401 (2011).
[9] Y. Wu, Y.-M. Lin, A. A. Bol, K. A. Jenkins, F. Xia, D. B. Farmer, Y. Zhu, and P. Avouris, Nature (London) **472**, 74 (2011).
[10] M. Y. Han, B. Ozyilmaz, Y. Zhang, and P. Kim, Phys. Rev. Lett. **98**, 206805 (2007).
[11] D. V. Kosynkin, A. L. Higginbotham, A. Sinitskii, J. R. Lomeda, A. Dimiev, B. K. Price, and J. M. Tour, Nature (London) **458**, 872 (2009).
[12] L. Jiao, L. Zhang, X. Wang, G. Diankov, and H. Dai, Nature (London) **458**, 877 (2009).
[13] S. S. Datta, D. R. Strachan, S. M. Khamis, and A. T. C. Johnson, Nano Lett. **8**, 1912 (2008).
[14] J. Campos-Delgado *et al.*, Nano Lett. **8**, 2773 (2008).

[15] X. Li, X. Wang, L. Zhang, S. Lee, and H. Dai, Science **319**, 1229 (2008).
[16] J. Cai *et al.*, Nature (London) **466**, 470 (2010).
[17] A. Mugarza, A. Mascaraque, V. Pérez-Dieste, V. Repain, S. Rousset, F. J. García de Abajo, and J. E. Ortega, Phys. Rev. Lett. **87**, 107601 (2001).
[18] V. Dose and G. Reusing, Applied Physics (Berlin) **23**, 131 (1980).
[19] G. Kresse and J. Hafner, Phys. Rev. B **47**, 558 (1993).
[20] G. Kresse and J. Furthmüller, Phys. Rev. B **54**, 11169 (1996).
[21] J. P. Perdew, K. Burke, and M. Ernzerhof, Phys. Rev. Lett. **77**, 3865 (1996).
[22] P. E. Blöchl, Phys. Rev. B **50**, 17953 (1994).
[23] G. Kresse and D. Joubert, Phys. Rev. B **59**, 1758 (1999).
[24] S. Grimme *et al.*, J. Comput. Chem. **27**, 1787 (2006).
[25] A. Varykhalov, J. Sanchez-Barriga, A. M. Shikin, C. Biswas, E. Vescovo, A. Rybkin, D. Marchenko, and O. Rader, Phys. Rev. Lett. **101**, 157601 (2008).